Photonic band-gap masks to enhance resolution and depth of focus

John Nistler, Koby Duckworth, Jiri Chaloupka[a], Matt Brock

Psida Lithography & Software LLC, info@psi-da.com, PO Box 571 Martindale, Texas 78655
a)Institute of Condensed Matter Physics, Faculty of Science,
Masaryk University, Kotlarska 2, CZ-61137 Brno, Czech Republic

Introduction

In the first part of 1990, the primary author and his colleagues at Advanced Micro Devices started to investigate the feasibility of Phase Shift Mask technology and Off axis illumination working off of the intial work of Dr. Levenson[1]. [2,3,4,5, 6,7] By 1991 in collaboration with Dr. Gregory Hughes of Dupont Photomask, Jim Wiley of KLA instruments, Jorge Freyer and Bob Nabor of Etec Systems, Dr. Eytan Barouch of Princeton University and Dr. Andrew Neurether of University of California at Berkeley; Advanced Micro Devices was able to produce first flash product utilizing multi-phase alternating aperture psm primarily due to the invention of the "voting technique" by the primary author[8] and the invention of the undercut etch by the primary author and Dr. Hughes. The voting technique was the only effective way of building defect free printing reticles for approximately the first 9 years of reticles being used in manufacturing.

Advanced Micro Devices under the guidance of the primary author proceeded with attenuated psm for contacts and AAPSM for the gate level whereas their primary competitor, other companies proceeded with the use of Rim PSM approaches. The one reason that Advanced Micro devices was able to obtain "defect free printing" masks at a time when defect repair was not feasible was primarily due to the combination of the "voting technique" and the undercut etch. The voting technique reduced defects to no greater than 60 degree phase defects whereas the undercut etch tended to reduce sharp edges creating a phase gradient that did not print within the +/- 20% wafer CD design criteria.

In general, the industry has proceeded with phase shift mask technology and off axis illumination but there have been certain manufacturing problems limiting the effectiveness as geometries became smaller.

The Attenuated PSM approach is limited in the k1 performance due to it being a "soft psm" effect. The Electric field does not necessarily have to go through zero thus neither does the intensity which is proportional to the electric field squared, $I \alpha E^2$. It has found extreme usefullness though because it does not require a complimentary exposure mask to eliminate phase transistions, requires typically only a single maskmaking pattern layer (this is not the case for tri-tone masks necessarily) and intensity oscillation around contact holes which create unwanted exposure of resist can be addressed by utilizing an absorbing dye in the resist. Improvements in the Attenuated PSM approach has included the addition of a Chome layer over the attenuated layer creating a tri-tone mask. Unfortunately as geometries continue to shrink, OPC generation is becoming more complex or does not address the diffraction effects of the corners. The use of tri-tone helps to address the difficulties with printing large contacts using an attenuated mask.

Emerging Lithographic Technologies XI, edited by Michael J. Lercel,
Proc. of SPIE Vol. 6517, 65171F, (2007) · 0277-786X/07/$18
doi: 10.1117/12.712295

The CAAPSM approach is the most commonly used "strong psm" effect type of reticle. This is a two mask exposure process where one reticle or field is either a Binary or Attenuated pattern and the second reticle or field is an AAPSM, alternating aperture phase shift mask. This reticle type was intially used primarily at gate mask, its most common use still today. Its early precursor the multi-phase reticle was more difficult to design but effective in producing "defect free printing" single exposure reticles for complex logic devices. [9,10] Even though it is extremely effective for printing geometries in production down to at least k1=0.35, the initial intensity imbalance caused by the actual 180 degree phase differance either do to etching or trenching the quartz or a deposited film creates a potential pitch walk effect as focus is changed. To adjust for this problem the undercut etch was designed to adjust the 3 dimensional image using Kane Yee's algorithmic approach for FDTD solution of Maxwell's equations.[11] Unfortunately the undercut reduces overall chrome or attenuated adhesion strength resulting in chrome peeling or fingers during reticle cleans or subsequeant processing. The second problem with the intensity imbalance is that smaller pitches even when using an undercut etch requires a different CD bias than larger pitches.[15] Various approaches such as the SCAA mask have been proposed but the added complexity of depostion in the mask shops and subsequent etching have not been well accepted. More recently the two mask/double exposure utilizing AAPSM or Attenuated reticles have been explored to extend basic optical resolution to k1 = 0.25. This approach utilizes a hardmask between the first and second exposure. The first exposure consists of exposing 1:3 ratio L/S patterns, then the second exposure pattern is aligned and placed between the initial patterns.[16] Of course alignment is extremely critical especially if drive currents of transistors in the same chain are done with the different exposures.

To print ever smaller contacts the AAPSM and Chromeless approach has been utilized in recent investigations into the phase vortex via approach.[17,18,19] The vortex phase mask consists of utilizing multiple phases of rectangular features to optimize for contacts. Similiar to the original work utilizing the Amoeba algorithm to optimize for contact printibility by the primary author, Dr. Yong Liu and Dr. Avideh Zhakor in the early 90's.[20] The primary difference is the use of inverse algorithmic approaches to optimize for the contact design. The manufacturability difficulties are still the same. Mask makers have difficulties in producing such small rectangles repetitively over a 6 inch mask with the type of control necessary to maintain a 15% exposure window and good depth of focus.

The Chromeless approach which is the strongest of the PSM approaches as far as effective depth of focus and contrast has found very little use in manufacturing primarily due to the difficulty of keeping the clear glass clean of particulate contamination. The Rim PSM approach even though attractive from a design perspective has effectively been dropped in manufacturing due to the difficulty of maintaining the tight CD criteria required for the small rim shifters.

The authors introduce initial simulation work on Photonic Bandgap Enhanced or PBE reticles that tends to address the manufacturing problems associated with typical PSM reticles while improving potential resolution capabilities to 35 and 25 nm utilizing 193 nm immersion lithography. The proposed approach for manufacturing reduces the overall defect issues associated with PSM approaches.

Discussion.

In 1968, Prof. Victor Veselago[21] first proposed that certain meta-materials could be made that would effectively look to electromagnetic waves traveling through the matierial that the electric permeativity and mangnetic permeability were both negative.

Recently the technique has been demonstrated in the microwave and radio frequency range using split ring resonators and wire gratings as individual layers. Photonic crystals have also been looked at for possible usage. Demonstartion that a photonic slab actually works as an improvement in Ez field propagation has been recently demonstrated using fluorescent polymers.[22] Therefore the theory and demonstration of theory shows that left handed optical materials will improve resolution and depth of focus by improvement of the electric field propagation in the near field. The authors propose that extension of Veselago's ideas with the theories and models developed for device physics dealing with the problem as a Photonic Bandgap Enhanced optical and x-ray approach further improves the practical modeling and manufacturability of the PBE materials.

The purpose of this paper is to first introduce the modeling methods necessary for designing high quality PBE materials for electromagnetic propagation. Note the term electromagnetic propagation can be taken in the literal sense. In this paper we discuss optics, but the modeling is also applicable to electric current propagation.

Second we will compare the PBE reticles to known PSM approaches used in nanolithography today and discuss some of the advantages associated with the new approach.

The actual discussion regarding the manufacturing of the PBE reticles will be reserved for another paper.

Basics of photonic band gaps

The easiest way to understand the behaviour of light in a photonic crystal is to compare it to the movement of electrons and holes in a semiconductor. In a silicon crystal, for example, the atoms are arranged in a diamond-lattice structure, and electrons moving through this lattice experience a periodic potential as they interact with the silicon nuclei via the Coulomb force. This interaction results in the formation of allowed and forbidden energy states. For pure and perfect silicon crystals, no electrons will be found in an energy range called the forbidden energy gap or simply the band gap. However, the situation is different for real materials: electrons can have an energy within the band gap if the periodicity of the lattice is broken by a missing silicon atom or by an impurity atom occupying a silicon site, or if the material contains interstitial impurities (additional atoms located at non-lattice sites).

Now consider photons moving through a block of transparent dielectric material that contains a number of tiny holes or nanotubes arranged in a lattice pattern that abruptly change in permitivity and permeability from the transparent dielectric material. As an example consider the situation of air holes in a silicon media utilizing light in the 635 nm range. The photons will pass through regions of high refractive index and absorbtion, the silicon - interspersed with regions of low refractive index - the air holes. To a photon, this contrast in refractive index looks just like the periodic potential that an electron experiences travelling through a silicon crystal. Indeed, if there is large contrast in refractive index between the two regions then most of the light will be confined either within the semiconductor material or the air holes. This confinement results in the formation of allowed energy regions separated by a forbidden region - the so-called photonic band gap. Since

the wavelength of the photons is inversely proportional to their energy, the patterned dielectric material will block light with wavelengths in the photonic band gap, while allowing other wavelengths to pass freely.

It is possible to create energy levels in the photonic band gap by changing the size of a few of the air holes in the material. This is the photonic equivalent to breaking the perfect periodicity of the silicon-crystal lattice. In this case, the diameter of the air holes is a critical parameter, together with the contrast in refractive index throughout the material.

Photonic band gap structures can also be made from a lattice of high-refractive-index material embedded within a medium with a lower refractive index. A naturally occurring example of such a material is opal. However, the contrast in the refractive index in opal is rather small, which results in a rather small band gap.

The potential of photonic-crystal structures was first realized in 1987 by Eli Yablonovitch, then at Bell Communications Research in New Jersey. A few years later in 1991, Yablonovitch and co-workers produced the first photonic crystal by mechanically drilling holes a millimetre in diameter into a block of material with a refractive index of 3.6. The material, which became known as "Yablonovite", prevented microwaves from propagating in any direction - in other words, it exhibited a 3-D photonic band gap. Other structures that have band gaps at microwave and radio frequencies are currently being used to make antennae that direct radiation away from the heads of mobile-phone users.

In spite of this success, it has taken over a decade to fabricate photonic crystals that work in the near-infrared (780-3000 nm) and visible (450-750 nm) regions of the spectrum. The main challenge has been to find suitable materials and processing techniques to fabricate structures that are about a thousandth the size of microwave crystals.

A rough estimate of the spacing between the air holes (or the lattice size) is given by the wavelength of the light divided by the refractive index of the dielectric material. The problem in making small structures is compounded because it is more favourable for a photonic band gap to form in dielectrics with a high refractive index, which reduces the size of the lattice spacing even further. For example, suppose we wanted to create a photonic crystal that could trap near-infrared light with a wavelength of 1 μm in a material with a refractive index of 3.0. We would have to create a structure in which the air holes were separated by about 0.3 μm - an extremely difficult task. If the scale was 1000 times smaller, we could build the structure atom-by-atom using a chemical reaction; and if it was 1000 times larger we could build the structure mechanically, as Yablonovitch and co-workers did.

To be able to create photonic crystals for optical devices, we need to use state-of-the-art semiconductor-microfabrication techniques with their associated high production costs and investment. For this reason computer modelling of prospective photonic-crystal structures is also a very important area of research, as it may prevent expensive fabrication errors later.

Simulation models.

Finite-difference time-domain (FDTD) is a popular computational electrodynamics modeling

technique. It is considered easy to understand and easy to implement in software. Since it is a time-domain method, solutions can cover a wide frequency range with a single simulation run. Since about 1990, FDTD techniques have emerged as a primary means to computationally model many scientific and engineering problems dealing with electromagnetic wave interactions with material structures. Current FDTD modeling applications range from near-DC (ultralow-frequency geophysics involving the entire Earth-ionosphere waveguide) through microwaves (radar signature technology, antennas, wireless communications devices, digital interconnects, biomedical imaging/treatment) to visible light (photonic crystals, nanoplasmonics, solitons, and biophotonics). The FDTD method used in this paper is specifically related to the grid and time-stepping algorithm proposed by Kane Yee.[11]

The FDTD method belongs in the general class of grid-based differential time-domain numerical modeling methods. Maxwell's equations (in partial differential form) are modified to central-difference equations, discretized, and implemented in software. The equations are solved in a leapfrog manner: the electric field is solved at a given instant in time, then the magnetic field is solved at the next instant in time, and the process is repeated over and over again.

When Maxwell's differential equations are examined, it can be seen that the change in the E-field in time (the time derivative) is dependent on the change in the H-field across space (the curl). This results in the basic FDTD time-stepping relation that, at any point in space, the updated value of the E-field in time is dependent on the stored value of the E-field and the numerical curl of the local distribution of the H-field in space. Unfortunately, this also means that using the FDTD method on larger problems can lead to significant computational times and memory increase especially if nanometer scale grids are necessary as is found in solving photolithography related problems. The approach therefore to deal with larger problems is to set up a periodic solution and use Perfectly Matched Layers, PML's, that are an artificial total absorbing material in the calculations.[12] Thus unrealistic reflections at interfaces is avoided. But this requires also a careful setup of the PML's to represent the problem, and the small grid still restricts the use of this method for large logic related problems where periodicity may not be represented in a small area. Therefore we have also evaluated a new method for dealing with photolithography related problems comparing it to the FDTD method.

A second method involves looking at expanding the concept of Bloch's Theorem to look at wave scattering of electromagnetic spectrum through periodic structures. At this time, the method is applicable for two dimensions, but looks promising for 3 dimensional representation. A Fourier expansion method assumes a system periodic in the X direction (period a) illuminated by a monochromatic plane wave. In the case of a non-periodic system, the supercell method is used to achieve an artificial periodicity. The electromagnetic field excited by the plane wave is a Bloch wave compatible with the X-periodicity of the system and Bloch vector determined by the angle of incidence and frequency of the illuminating wave. By introducing infinitesimally thin horizontal air spacers at convenient Z positions $\{z_j\}$, the system is divided into a set of blocks and dealt with using the transfer matrix method reducing overall computational time. In the spacers, the electromagnetic field can be described as a superposition of upwards and downwards propagating plane waves $E_y(x,z)=\sum \exp(i k_x^{(n)} x)[E_j^{(n,up)}\exp(i k_z^{(n,up)}(z-z_j))+E_j^{(n,down)}\exp(i k_z^{(n,down)}(z-z_j))]$ with the wavevectors with the X components equal to $k_x^{(n)}=k_x+2\pi n/a$ and with Z components chosen according to $|\boldsymbol{k}^{(n)}|=\omega/c$. The intensities of the plane waves $E_j^{(n)}$ at different interfaces are

related by the transfer matrices of the blocks. We use the plane wave expansion method to calculate these transfer matrices.[13] The transfer matrix of the whole system is constructed from the transfer matrices of the individual blocks using the S-matrix algorithm. [14]
In a practical realization of the method, the number of Fourier components has to be restricted to N_{max} which limits the wavefield resolution in the X-direction. Since the algorithms involve matrix operations like inversion or matrix multiplication, the computational time scales as N_{max}^3. This nonlinear scaling presents the limitation of the method in terms of a/λ, but for moderate values of this parameter the performance can be much better than by the FDTD method where the computational time scales cubic with the X, Y and Z-resolution. As an example using the FDTD method a reduction from a 10 nm to 1nm per side of the cubic grid translates into a 1000 times increase in the number of computational nodes.

Simulation Setup.

The simulations consisting of evaluating Te polarization illuminated reticles thus avoiding the issue with Te/Tm variations associated with pitch published earlier.[22] Initially we first evaluated the basic design aspect of an idea we have in relation to making of the photonic bandgaps in improving reticle design over the existing PSM and off-axis illumination techniques. Our first pass at design was a basic screening test to understand a) if the technique was feasible, and b) what were the important design parameters and how would it impact our basic process flow.

The conditions for simulation of the initial screening setup are indicated in Table 1. Only near field results are reviewed so that only true improvements in the actual electric field and illumination process of the different techniques are compared. This method proved effective when first evaluating PSM in the early 90's and is used now to look at the potential fundamental improvements seen in the PBE technique. Even though the PSIDA_3D mask code can handle full 3 dimensional masks, the y-plane is kept at 1 nm allowing comparison to the new Bloch Wave Fourier Expansion Method.[23]

Table 1.

Wavelength: 248 nm Reduction:4 Chrome thickness: 750 nm
Phase Trench Depth: 0.2439 μm

Wavelength: 193 nm Reduction:4 Chrome thickness: 750 nm
Phase Trench Depth: 0.17209 μm

Types of reticles compared: AAPSM and PBE.
1X feature sizes from 150 nm to 30 nm were reviewed during initial screening.
Undercut X-dimension ranged from 0 to 25 nm. (Only on the AAPSM)
Nanotube diameters in the PBE reticle ranged from 15 to 140 nm (4X dimensions)

Initial Screening Test Simulation Results.

In Figure 1, a basic AAPSM layout of a 180 nm equal line/space pattern is shown as a referance.

The illumination results with and without the undercut etch indicated in Figure 1 is shown in Figures 2 and 3. Note that the etched or trenched quartz area of the AAPSM mask is smaller in actual illumination width on the left side of the graphs. Even undercut etches are limited in their abilities to adjust for the difference in CD between adjacent spaces and line biasing is typically used to account for the difference. During the initial screening experiment we did not include line biasing per edge.

In actual manufacturing this line bias along with the effects of proximity influence distance can significantly increase the design data, especially if a significant amount of the hierarchy has to be flattened.

Figure 1. Note in this case for 180 nm AAPSM Line/Space mask, an undercut etch is indicated. This specific mask is actually used for Figure 3. Mask thickness indicated in dark blue is 1000 Angstroms in width. Actual chrome/glass interface is at 0.58 while the chrome/air interface is at 0.48 on the Z scale. Y dimension goes into the page and is on the order of 10 nm. The trench depth is designed for 248 nm exposure. The same chrome width is used throughout the initial studies

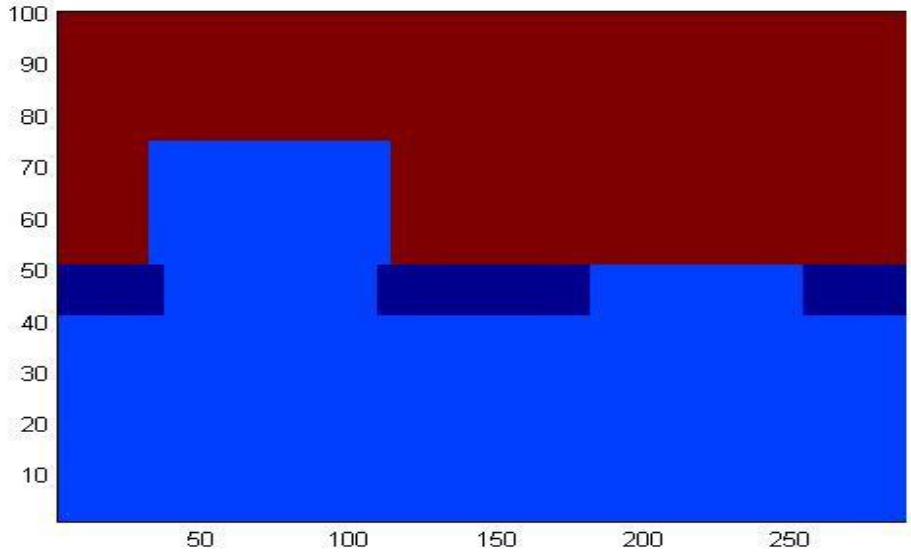

Figure 2: The simulation results for the 180 nm Line/Space (1X) pair indicated in Figure 1, but no undercut etch is used. The quartz etch sidewall in this case was 90 degrees and was on edge with the chrome edge. The actual mask used for the simulations is 4X, i.e., the openings for the space/line/space is 720 nanometer.Note that it is clear that the left, etched trench area is smaller than the intensity indicated on the right of this 180 nm AAPSM.
Bibliography

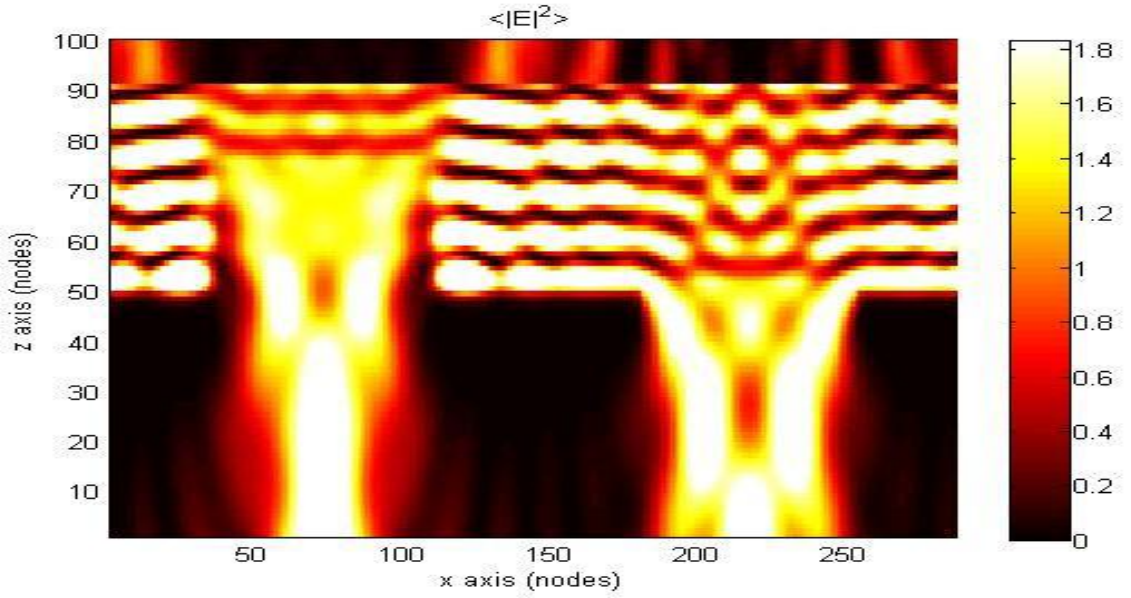

Figure 3. Intensity distribution incorporating the undercut etch indicated in Figure 1 for the same 180 nm (1X) space/line/space. Note that the left image is still slightly undersized and there is a definate taper to the left image effectively reducing the dof of the trench area well below what would normally be calculated using only Kirchoff or Abbe thin mask approximations.

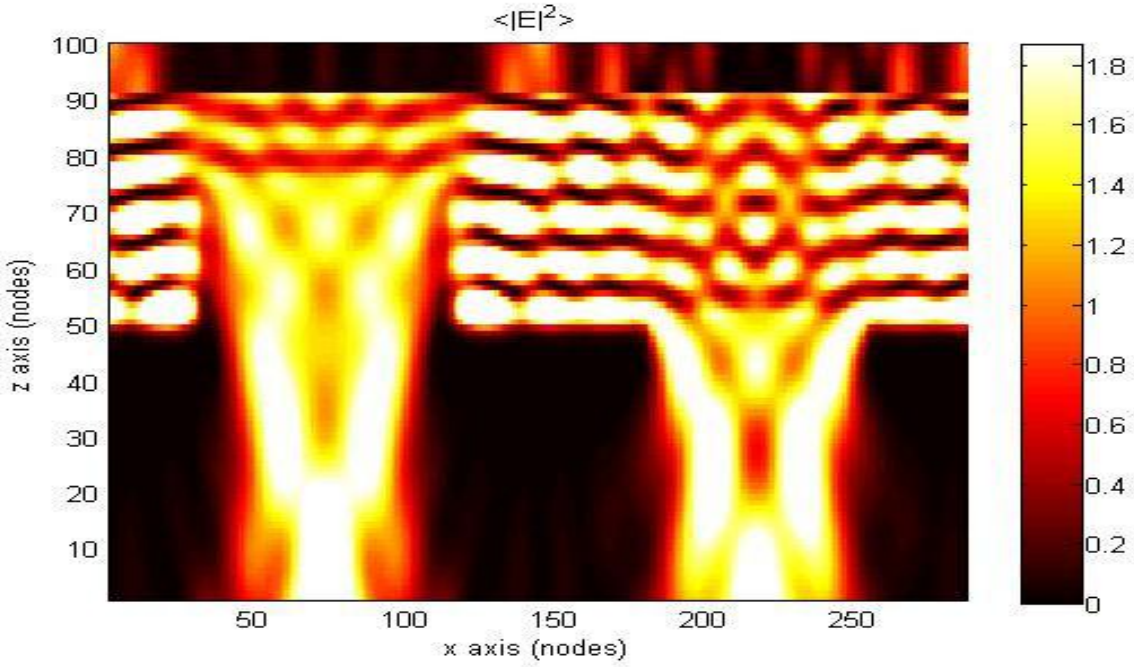

Figure 4. The intensity distribution for a 140 nm (1X) space/line/space is shown for the PBE mask

incorporating the company's Photonic Bandgap intellectual properties. The same process was utilized to simulate 180 to 120 nm equal Line/Space. The mask involves no undercut etch and could be processed utilizing a single resist coat. In fact the normal resist strip, CD adjustment, inspection of the attenuated or chrome film and repair could be utilized in this approach.

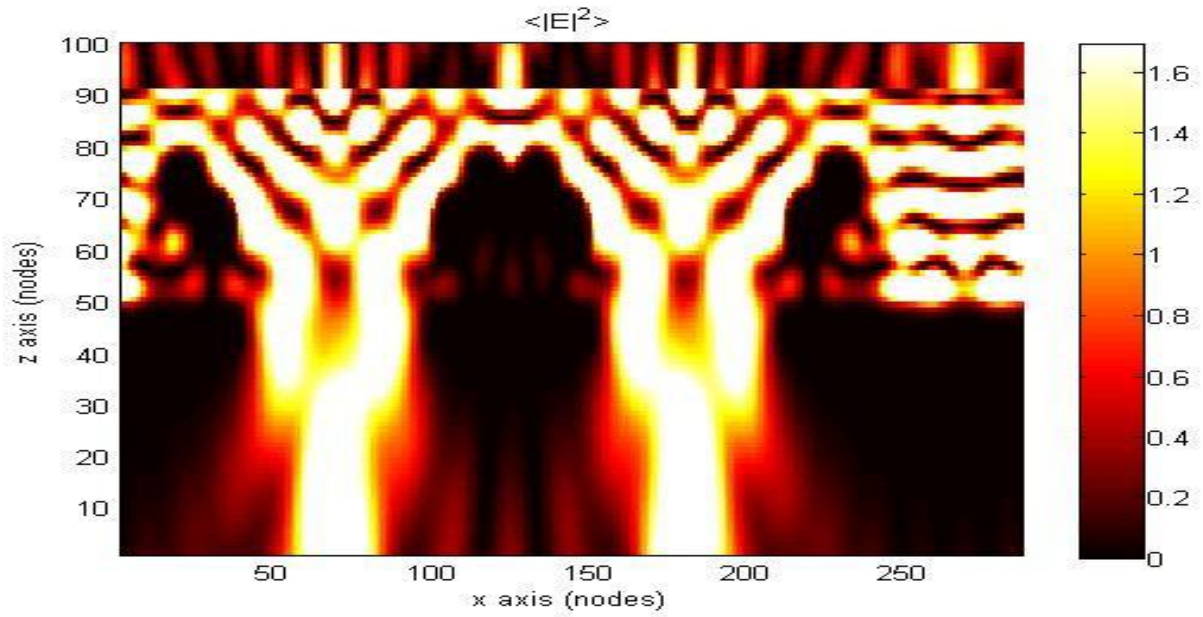

Note that in Figure 2 and 3 the simulation results well represent the known results for the AAPSM with and without undercut etch utilizing the Kane Yee algorithmic approach to solving Maxwell equation problems. Utilizing this same algorithmic approach therefore seems feasible for evaluating the potential benefits associated with Photonic Bandgap Enhanced or PBE reticles.

Further exploring the ability to properly design resolution extensions during the initial screening simulations, the authors looked at extending resolution using 193 nm illumination to at least a 30 nm line/space 1X feature size.

Some 1X critical dimension difference for the same mask CD was noticeable between dense, semi-dense and isolated features during the intial screening test. Further evaluation indicates that properly optimized design helps to reduce this effect.

Figure 6. A 80nm space, 100 nm line and 80 nm space in a dark field mask at 248 nm illumination. Note that the intensities from the two spaces are still extremely bright, and very sharp in contrast. The mask exit pupil is at Z=42.

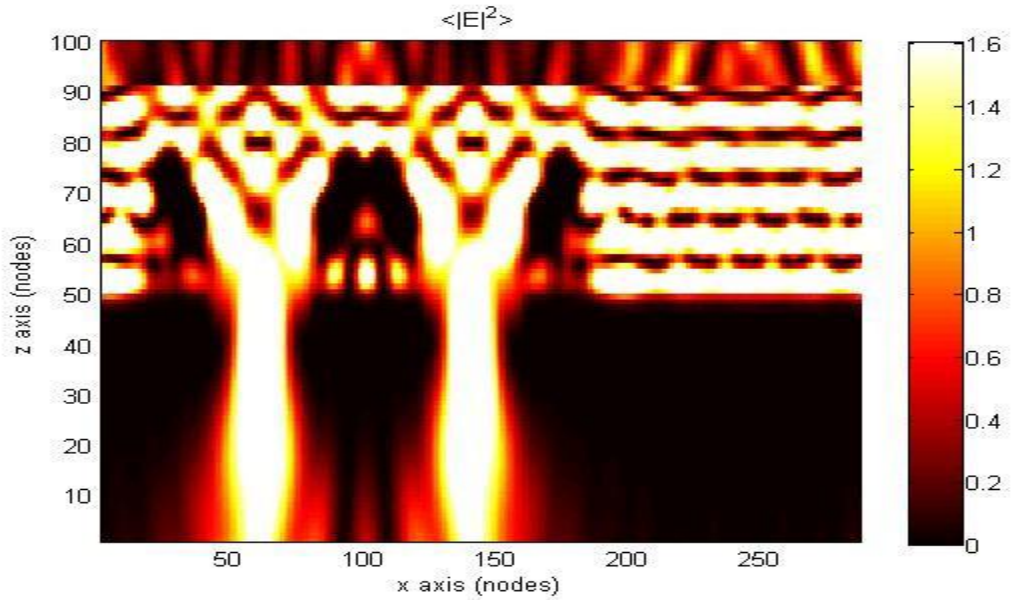

Figure 7. Equal line/space at 80 nm for a 248 nm exposure! No real optimization was incorporated to reduce dense, semi-dense and isolated critical dimension differances.

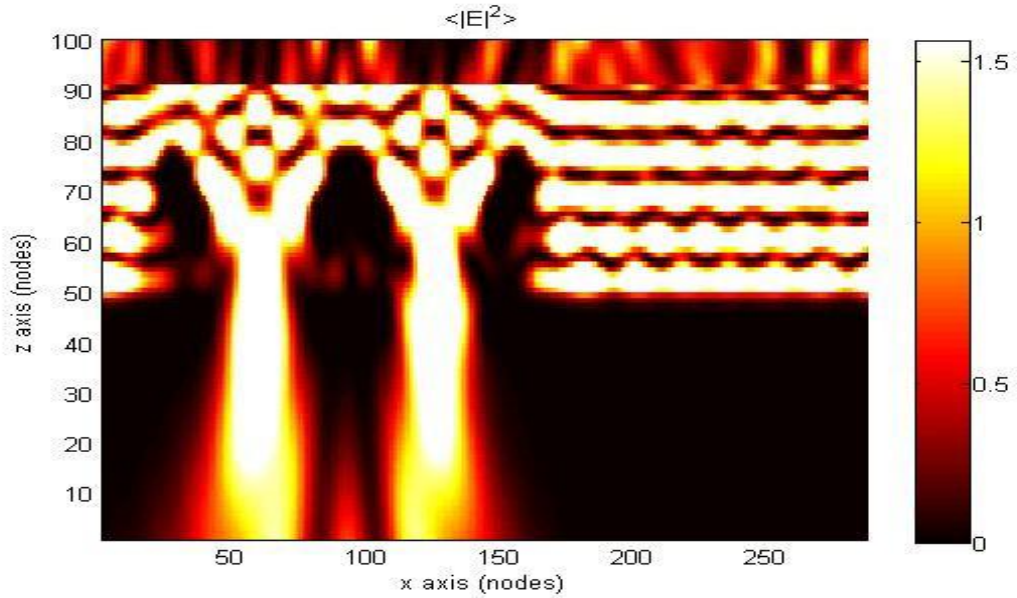

We will now switch to 193 nm T E polarized illumination. The same basic space/line/space binary dark field mask is the starting point prior to manufacturing the PBG. In Figure 8 it is demonstrated that 80 nm equal line space can be accomplished. Not a significant effort to optimize for 80 nm was done because of the interest in looking at 45 nm and below. Figure 8 indicates the results for the 30 nm half pitch space/line/space utilizing a 193 nm T E polarized illumination normal to the

mask plane as in a circular illuminator.

Figure 8. 30 nm half pitch using 193 nm T E polarized illumination. The chrome/air interface is at Z=48.

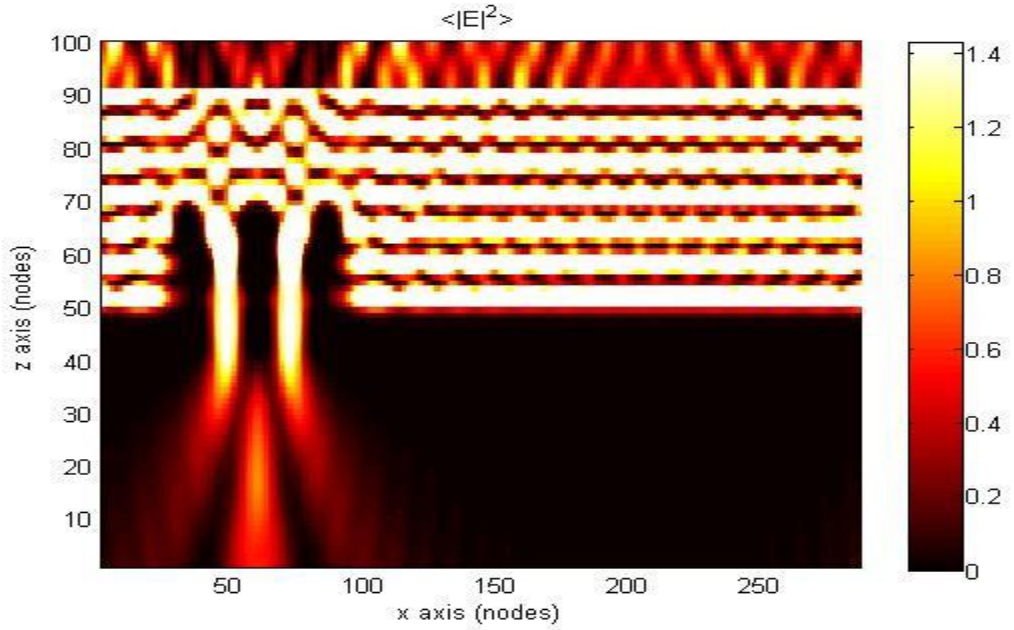

Note that the images are still relatively square at Z=42 with no taper and immediately around the chrome openings the electromagnetic propagation in the chrome is completely eliminated.

Thus during the initial simulation screening the potential to utilize the PBE reticle technique to enhance resolution was demonstrated. Further evaluation was started to look at the overall manufacturing and defect related issues discussed in the manufacturability evaluation.

Aerial Image Near field comparison to Phase shift masking.

In this study we looked at the near field imaging capabilities of the Photonic Bandgap Enhanced, PBE, reticles versus the commonly known AAPSM and Rim PSM approaches. The basic study is as shown in Figure XX looking at W1 and W2 of the two adjacent spaces. As is known, even with a undercut etch in the trench etched region of the AAPSM of 20 nm per side there is still up to 7 nm difference between the two spaces. The Rim phase shifted mask did show balance between both spaces but had no near field imaging capabilities below 80 nm equal line/space using 193 nm illumination. Even if biasing is used for the AAPSM the smallest resolution of the near field image using 193 nm is at 65 nm. It is an important point to keep in mind that even if high index of refraction liquids are used in immersion lithography there still has to be an initial near field image to work from.

The PBE reticle demonstrates near field imaging capabilities for equal line/space using 193 nm down to 25 nm. Note that to obtain 25 nm, some design criteria had to be adjusted. It was also

noted that the PBE material could effectively be modified across the reticle to account for birefrigence or transistor length modifications.

Figure 9A. Near field aerial image simulation results at 193 nm T_E illumination. Critical dimenisons are at 1X values.

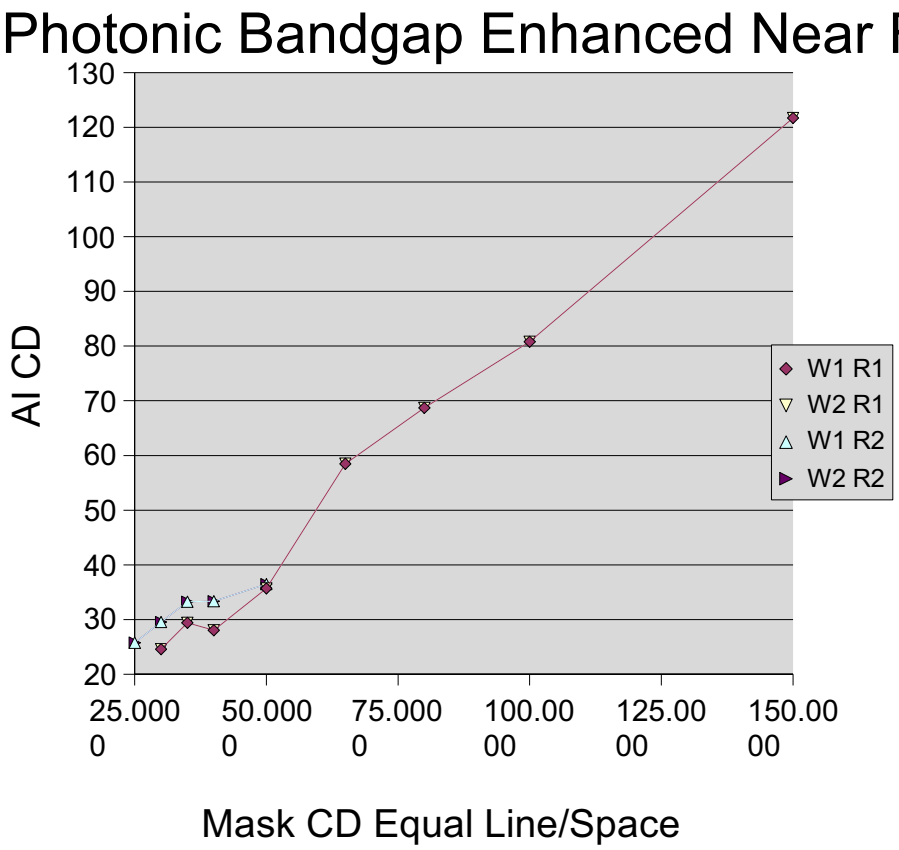

Figure 9B. Near field aerial image simulation results at 193 nm T_E illumination. Critical dimenisons are at 1X values. The AAPSM undercut used was 20 nm, but at 125 nm resolution and below any practical undercut used still does not correct the near field W1 versus W2 bias.

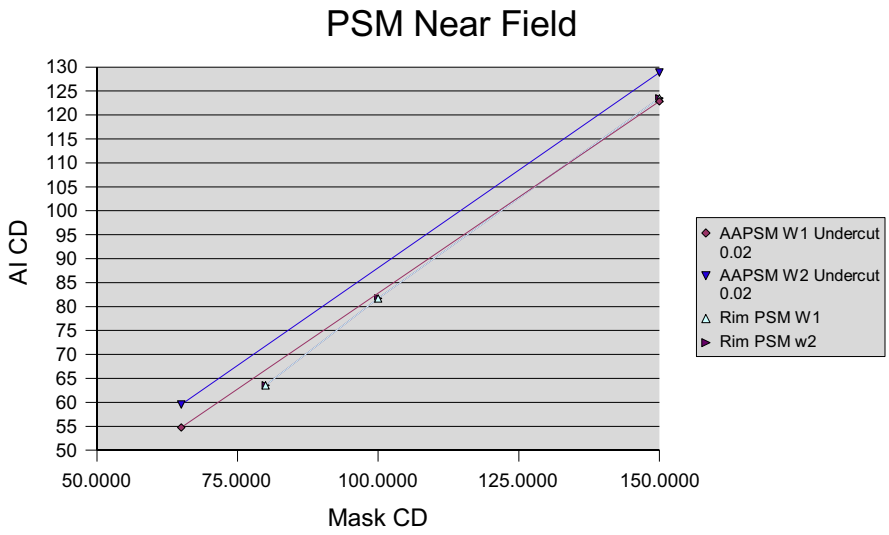

Summary.

A new concept, photonic bandgap enhanced , PBE reticles is introduced. The technique was simulated utilizing 4X reduction reticles and predicting the 1X near field imaging that was produced. Using 193nm TE illumination and PBE, Photonic Bandgap Enhanced, reticles indicate through simulation the ability to produce image capabilities at least to 25 nm. Comparisons through the same simulation tools were made to existing PSM techniques which are only capable of producing down to 65 nm near field images.

Modeling approaches consisted of using Kane Yee's algorithmic FDTD method and a new concept in modeling of Maxwell's equations which leads to reduced computational time, but is especially beneficial in optimization techniques for evaluating best methods for manufacturing of the PBE material.

Significant control in image balancing between spaces is indicated plus a manufacturable approach for validating the results has been indicated. The technique of PBE reticles looks very promising for decreasing overall manufacturable geometries in immersion lithography capabilities.

Acknowledements.

The authors would like to thank Dr. Andrew Neurether and his group at UC at Berkeley and Prof. Dr. Josef Humicilek of the Institute of Condensed Matter Physics at Masaryk University.

Bibliography

- 1) Phillip J. Brock etal. SPIE Vol. 1463, p. 87-100 (1991)
- 2) Steven K. Dunbrack etal. SPIE Vol. 1464, p. 314-326 (1991)
- 3) John L. Nistler etal. SPIE Vol. 1604, p. 236-264 (1992)
- 4) Chris A. Spence etal. SPIE Vol. 2197, p. 302-313 (1994)
- 5) John L. Nistler etal. SPIE Vol. 2254, p. 78-92 (1994)

- 6) Herschel M. Marchman etal. SPIE Vol. 2322, p. 360-373 (1994)
- 7) Chris A. Spence etal. SPIE Vol. 3236, p. 228-242 (1997)
- 8) John L. Nistler. US Patent # **5,308,722 May 3, 1994**
- 9) Paul W. Ackmann etal. SPIE Vol. 3051, p. 384-390 (1997)
- 10) Paul W. Ackmann etal. SPIE Vol. 3051, p. 146-153 (1997)
- 11) Kane Yee . IEEE Transactions on Antennas and Propagation **14**: 302–307. (1966)
- 12) J. Berenger . Journal of Computational Physics **114**: 185–200. (1994)
- 13) Kazuaki Sakoda, Phys. Rev. B, Vol. 51, p. 4672 (1995)
- 14) Lifeng Li, J. Opt. Soc. Am. A, Vol. 13, p. 1024 (1996)
- 15) C.A. Spence etal. SPIE Vol. 4066, p. 650-660 (2000)
- 16) Takeaki Ebihara etal. SPIE Vol. 5256, p. 985-994 (2003)
- 17) Marc David Levenson etal. SPIE Vol. 5256, p. 93-102 (2003)
- 18) Marc D. Levenson, Grace Dai, Takeaki Ebihara. Proc. SPIE Vol. 4889, p. 1293-1303 (2002)
- 19) Marc D. Levenson etal. Proc. SPIE Vol. 5377, p. 1237-1246 (2004)
- 20) Yong Liu etal. SPIE Vol. 1674, p. 44-52 (1992)
- 21) V. G. Veselago, Sov. Phys.-Solid State 8, 2854 (1967).
- 22) Robert J. Moerland and Niek F. van Hulst. 7 March 2005 / Vol. 13, No. 5 / OPTICS EXPRESS 1604
- 23) Jiri Chaloupka, Diploma Thesis: Wave Scattering in Photonic Crystals, Faculty of Science, Masaryk University. Brno, Czech Republic (March 14, 2005).